AGU PUBLICATIONS

Geophysical Research Letters

RESEARCH LETTER
10.1002/2016GL071879

Key Points:
- We used laboratory testing to simulate the effects of earthquake sequences of different character on landslide shear strength and behavior
- Ground shaking that does not cause high strain accumulation in landslides can increase bulk density in ductile hillslope materials
- This increases interparticle contact and so strengthens a landslide, reducing susceptibility to subsequent seismicity

Supporting Information:
- Supporting Information S1

Correspondence to:
M. J. Brain,
matthew.brain@durham.ac.uk

Citation:
Brain, M. J., N. J. Rosser, and N. Tunstall (2017), The control of earthquake sequences on hillslope stability, *Geophys. Res. Lett.*, *44*, doi:10.1002/2016GL071879.

Received 8 NOV 2016
Accepted 10 JAN 2017
Accepted article online 11 JAN 2017

The control of earthquake sequences on hillslope stability

Matthew J. Brain[1], Nick J. Rosser[1], and Neil Tunstall[1]

[1]Department of Geography and Institute of Hazard Risk and Resilience, Durham University, Durham, UK

Abstract Earthquakes trigger landslides in mountainous regions. Recent research suggests that the stability of hillslopes during and after a large earthquake is influenced by legacy effects of previous seismic activity. However, the shear strength and strain response of ductile hillslope materials to sequences of earthquake ground shaking of varying character is poorly constrained, inhibiting our ability to fully explain the nature of earthquake-triggered landslides. We used geotechnical laboratory testing to simulate earthquake loading of hillslopes and to assess how different sequences of ground shaking influence hillslope stability prior to, during, and following an earthquake mainshock. Ground-shaking events prior to a mainshock that do not result in high landslide strain accumulation can increase bulk density and interparticle friction. This strengthens a hillslope, reducing landslide displacement during subsequent seismicity. By implication, landscapes in different tectonic settings will likely demonstrate different short- and long-term responses to single earthquakes due to differences in the magnitude, frequency, and sequencing of earthquakes.

1. Introduction

In mountainous regions, large earthquakes can trigger widespread landsliding [*Keefer*, 1994]. In addition to causing extensive socioeconomic disruption [*Marano et al.*, 2010], earthquake-induced landslides play a key role in the evolution of mountain landscapes, increasing sediment flux through the fluvial network [*Dadson et al.*, 2004; *Hovius et al.*, 2011] and contributing to net erosion rates [*Marc et al.*, 2015; *Parker et al.*, 2011; *Robinson et al.*, 2016]. While earthquake ground shaking triggers near-instantaneous landsliding [*Li et al.*, 2014], some slopes do not fully fail and are weakened [*Khattak et al.*, 2010], resulting in elevated susceptibility of hillslopes to landsliding during postseismic rainfall [*Lin et al.*, 2008] and subsequent seismicity [*Parker et al.*, 2015]. These legacy effects have been broadly attributed to landscape-scale weakening of hillslope substrates resulting from increased brittle (micro)fracturing and joint dilation ("damage") caused by transient hillslope stresses experienced during earthquake ground shaking [*Wang et al.*, 2004]. Our understanding and interpretation of the behavior of brittle landslides in response to seismicity has a firm theoretical basis [*Petley et al.*, 2005].

In contrast, the response of ductile hillslope materials, and in particular if and how shear strength varies in response to repeat ground-shaking events of different character, is less well constrained. In turn, we cannot fully explain observations of the rates of postseismic landsliding in all settings [cf. *Parker et al.*, 2015]. This limits our ability to project the stability of ductile hillslopes into the future both in terms of the short-term effects of single earthquakes and the longer-term nature of net topographic change during and following earthquakes in different tectonic settings [*Keefer*, 1984; *Marc et al.*, 2016]. The aim of this paper is to assess if and how different sequences of ground shaking influence hillslope stability and landslide displacement in ductile hillslope materials prior to, during, and following an earthquake mainshock.

2. Methods and Experimental Approach

We used a novel geotechnical laboratory testing approach to address our aim. We undertook our testing program using a Dynamic Back-Pressured Shearbox (DynBPS) (plan dimensions: 100×100 mm; depth: 20 mm), which simulates earthquake ground-shaking conditions at a landslide shear surface [*Brain et al.*, 2015]. We completed a total of 17 tests (7 monotonic, 10 dynamic) on a silt material (see Table S1 in the supporting information), remolded to minimize variability in shear behavior resulting from sedimentary structure, stress history, and disturbance during sampling [*Burland*, 1990]. This allowed us to consider how shear strength evolves from a uniform baseline condition. During all tests, we monitored shear strain, ε_s; shear stress, τ; normal strain, ε_n; and pore water pressure, u (see Text S1 in the supporting information).

Our testing program had three stages. In the first stage, we used standard geotechnical procedures [*Head and Epps*, 2011, 2014] to characterize the baseline monotonic direct shear behavior of the sediment under drained conditions (strain rate = 0.1% min^{-1}) under normal effective stress (σ'_n) values of 50 kPa, 100 kPa, and 150 kPa. This allowed us to determine the general rheology and strength properties of the sediment (Figures 1a and 1b). This was required to define appropriate baseline stress conditions and stress amplitudes used during subsequent dynamic testing.

In the second stage, we undertook an additional four (and so a total of five) monotonic direct shear tests where $\sigma'_n = 100$ kPa (strain rate = 0.1% min^{-1}). We calculated the mean and standard error of τ and ε_n for each value of ε_s to define envelopes of baseline stress-strain and volumetric behavior (Figure 1c).

In the third stage, we undertook dynamic testing to determine the response of the sediment to earthquake loading at $\sigma'_n = 100$ kPa. In this stage, we undertook strain-controlled (0.1% min^{-1}) monotonic shear under drained conditions to specific values of ε_s and τ (Figure 1b). This simulated aseismic (static) shear stress in a hillslope and served as the baseline shear stress datum for the stress-controlled dynamic stage(s) of each test.

We simulated two dynamic loading scenarios indicative of "low-magnitude" and "high-magnitude" ground-shaking events (Figures 1d and 1e). These scenarios were intended to simulate loading conditions experienced by hillslopes during earthquakes of different character. Peak amplitudes during the low-magnitude and high-magnitude loading scenarios were selected on the basis of baseline (static) shear stress conditions relative to the Mohr Coulomb failure envelope (Figure 1b). The high-amplitude stress amplitude (±20 kPa) was sufficiently high to result in unstable dynamic stress states that lie "above" the failure envelope for all baseline shear stress and shear strain values used in dynamic tests. In contrast, the lower peak shear stress amplitude (±10 kPa) in the low-magnitude scenario did not result in unstable stress states in all baseline shear stress and shear strain values used in dynamic tests (Figure 1b). The peak amplitude (±10 kPa) in the low-magnitude scenario operates for fewer cycles than the peak amplitude (±20 kPa) in the high-magnitude scenario. In addition, the higher-frequency loading in the high-magnitude scenario was specified to encourage prolonged undrained loading (elevated pore water pressures). We specified a longer duration in the low-magnitude tests to increase the number of cycles operating under stable stress conditions. In contrast, the shorter duration specified for the high-magnitude loading scenario was used to avoid liquefaction failure, which would not have permitted assessment of the ongoing shear deformation of interest in this study.

Since lower magnitude ground-shaking events are more common in nature [*Gutenberg and Richter*, 1954], we ran each low-magnitude scenario as a sequence of 20 events, reestablishing baseline stress conditions between dynamic stages to replicate a constant slope angle and geometry. Following completion of the dynamic stage(s), we immediately reestablished baseline stress conditions and subsequently sheared the samples under strain control (0.1% min^{-1}) until $\varepsilon_s = 20\%$. We compared the results of our dynamic testing program to the baseline τ and ε_n envelopes to assess whether differences in strength and/or behavior occurred (manifest as deviations away from that observed during baseline monotonic tests), how long these effects persisted, and to explain any changes in behavior.

3. Baseline Shear Behavior

Stress-strain curves (Figure 1a) indicate that the sediment has a ductile rheology; shear stress, τ, increased until $\varepsilon_s \approx 3$–5% before stabilizing ($\sigma'_n = 150$ kPa) or only gradually increasing ($\sigma'_n = 50$ kPa and $\sigma'_n = 100$ kPa). During shearing, all samples continued to compress until ε_s reached approximately 10%. At greater values of ε_s, samples remained at near-constant volume or dilated very slightly (Figure 1a). We recorded peak τ values of 34.2 kPa ($\sigma'_n = 50$ kPa), 51.4 kPa ($\sigma'_n = 100$ kPa), and 65.6 kPa ($\sigma'_n = 150$ kPa), allowing us to define the Mohr Coulomb failure envelope (Figure 1b). The five monotonic direct shear tests undertaken at $\sigma'_n = 100$ kPa showed highly similar stress-strain and volumetric behavior (Figure 1c).

4. Low-Magnitude Shaking Sequences

We assessed the effects of a sequence of 20 low-magnitude shaking events on shear strength. We undertook four tests; in each, we monotonically sheared the sample to a different shear strain datum prior to dynamic loading: $\varepsilon_s = 1\%$ ($\tau \approx 32$ kPa); $\varepsilon_s = 2\%$ ($\tau \approx 40$kPa); $\varepsilon_s = 3\%$ ($\tau \approx 44$kPa); or $\varepsilon_s = 4\%$ ($\tau \approx 45$ kPa)

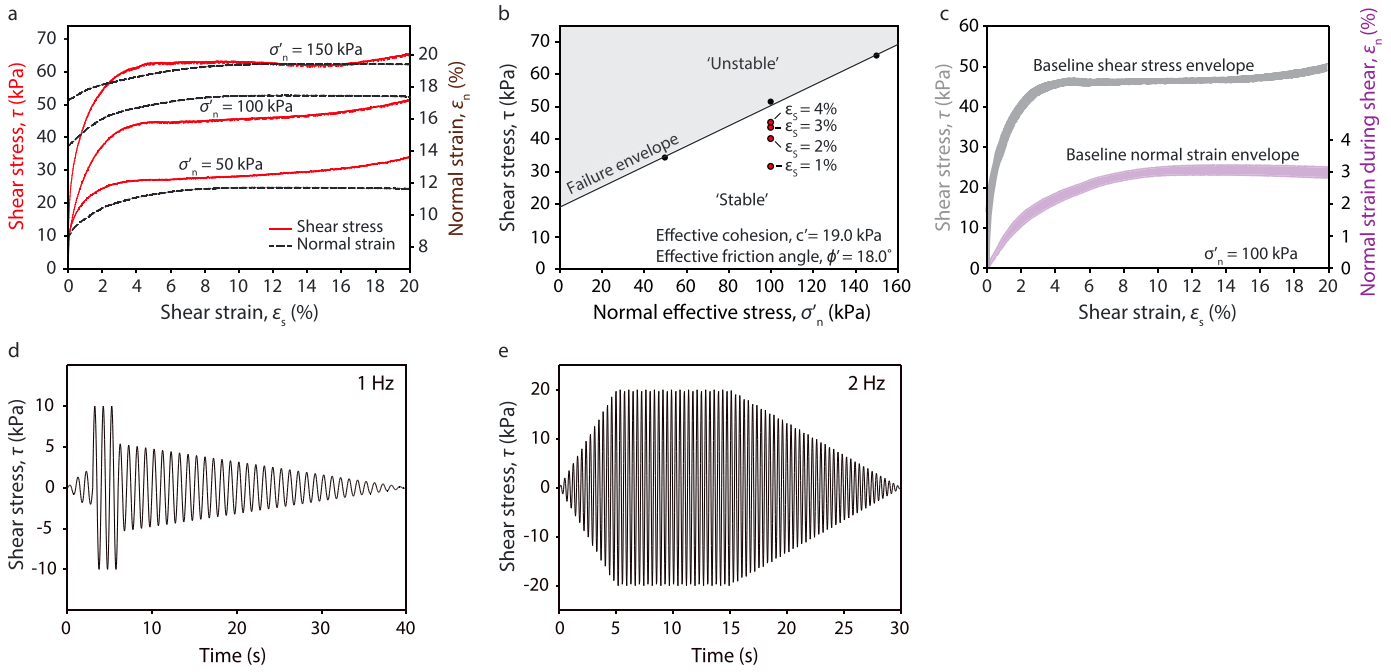

Figure 1. (a) Shear strain and volumetric behavior of sediment samples during strain-controlled monotonic direct shear under normal effective stress (σ'_n) values of 50, 100, and 150 kPa. (b) Peak strength Mohr Coulomb failure envelope based on monotonic test results (black circles). Red circles indicate baseline shear stress conditions at specified shear strains, as used in the dynamic tests. (c) Baseline shear stress and volumetric behavior envelopes during monotonic direct shear testing (σ'_n = 100 kPa). Shown are the dynamic shear stress time histories used in our (d) low-magnitude and (e) high-magnitude ground-shaking scenarios. In each dynamic test, these scenarios were applied relative to a specified shear stress datum, as indicated in Figure 1b.

(Figure 1b). Example results for tests where initial ε_s = 2% and 4% are displayed in Figure 2. Total ε_s accumulated following completion of the 20 dynamic events increased with the baseline values of ε_s and τ, though substantially greater strain accumulated where baseline ε_s = 3% and 4% (Figure 3a). In these tests, baseline shear stresses were sufficiently close to unstable stress states to permit shear strain accumulation (Figure 1b). Where initial ε_s = 3% and 4%, strain accumulation in each cycle did not systematically increase or decrease (Figure 3b).

Baseline stress states for tests where initial ε_s = 1% and 2% did not enter unstable stress states during dynamic loading. The magnitude of strain accumulation decreased with each shaking event in tests where initial ε_s = 1% and 2%. By event 20, the cyclic strain increment had reduced by 2 orders of magnitude to <0.01% per cycle (Figure 3b). This strain hardening can be explained by the evolution of ε_n during the dynamic loading stages. In tests where initial ε_s = 1% and 2%, τ amplitudes were insufficient to cause instability and generate large shear-strain accumulation; the sediment densified relative to baseline ε_n behavior, causing greater particle interlocking and increased frictional strength (Figures 2a–2d). The effects of this sediment densification are evident in postdynamic monotonic shear behavior; where ε_s accumulation was minimal and dynamic loading caused progressive densification (initial ε_s = 1% and 2%), τ required to shear the sediment subsequently increased relative to baseline values, which we describe as $\Delta\tau$ (Figure 2b). This postdynamic strengthening persisted, (Figure 2a) because the sediment appears to retain "memory" of this densification relative to monotonic loading conditions (Figure 2c). This effect is related to strengthening during dynamic loading; the greater the degree of densification and strengthening, the more persistent the enhanced shear strength (Figure 3c).

Where initial ε_s = 3% and 4%, densification during dynamic loading did not occur because the baseline τ condition in these tests was closer to the failure envelope, τ amplitudes were sufficient to cause prolonged instability and deformation, and undrained loading may also have prevented consolidation. The ε_n behavior in this test was similar to that displayed by the baseline ε_n envelope (Figures 2g and 2h). We observed no change in shear strength following completion of the dynamic stages relative to baseline behavior (Figures 2e and 2f).

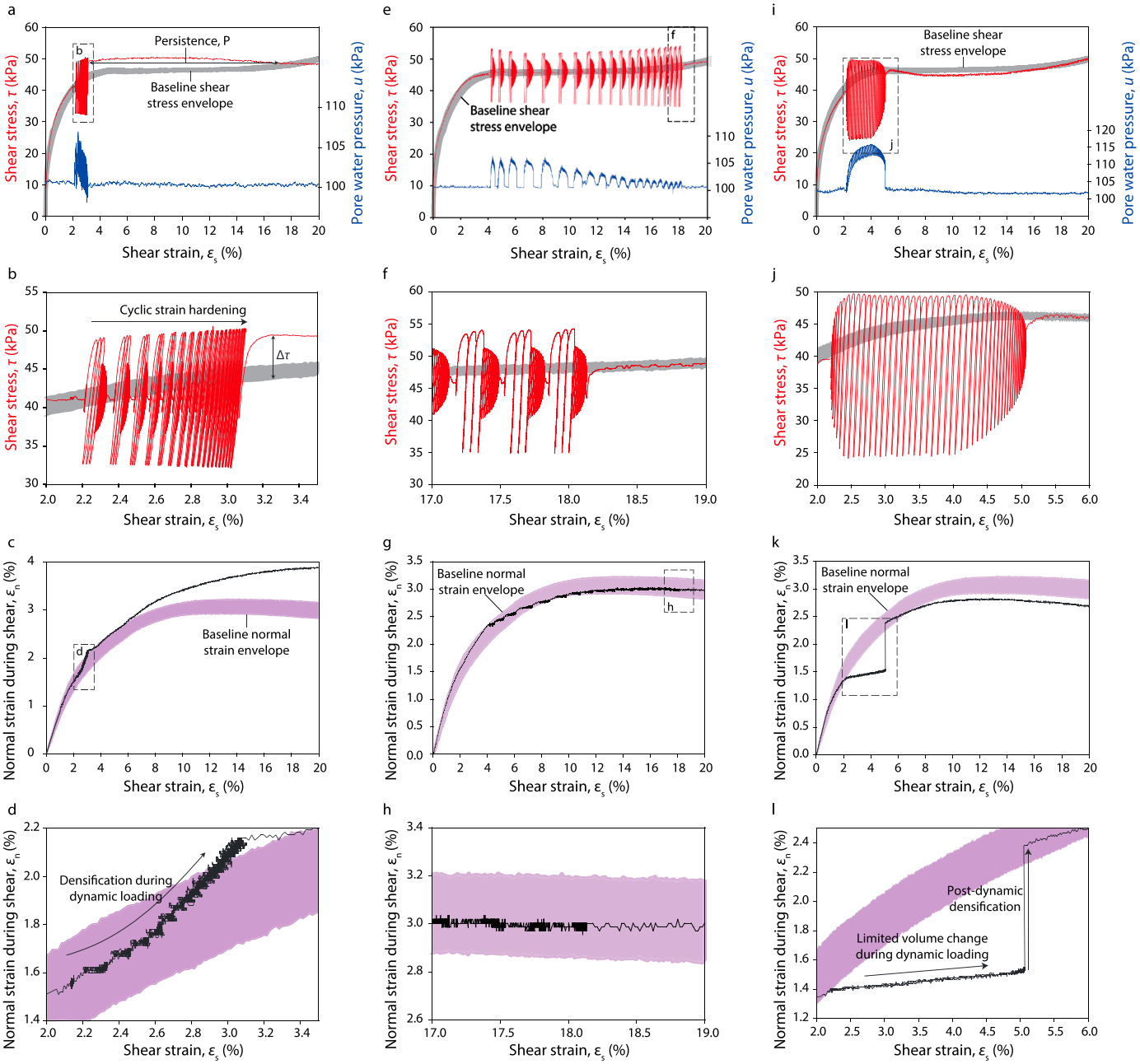

Figure 2. Example results demonstrating key elements of the dynamic shear testing program. Test data are organized in columns: (a–d) Results for behavior before, during and following 20 low-magnitude ground-shaking events where initial shear strain, ε_s, = 2%; (e–h) results for behavior during and following 20 low-magnitude ground-shaking events where initial $\varepsilon_s = 4\%$; (i–l) results for behavior during and following a single high-magnitude ground-shaking event where initial $\varepsilon_s = 2\%$. From the top, the first row displays stress-strain and pore pressure behavior; detail of the dynamic and immediate postdynamic behavior is displayed in the second row. The third row displays volumetric behavior during dynamic shearing, with further detail displayed in the zoomed-in figures in the fourth row.

5. High-Magnitude Shaking Event

We explored the effect of a single high-magnitude shaking event on shear strength and behavior. We again undertook four tests; in each, we monotonically sheared the sample to a different datum of ε_s: 1% ($\tau \approx 32$ kPa); 2% ($\tau \approx 40$kPa); 3% ($\tau \approx 44$kPa); and 4% ($\tau \approx 45$ kPa) (Figure 1b). Example results for tests where initial $\varepsilon_s = 2\%$ are displayed in Figure 2. Greater baseline values of τ resulted in increasing ε_s during the dynamic stage, though the differences between tests are minimal, particularly where $\varepsilon_s = 2\%$, 3%, and 4% (Figure 3a). Pore water pressure, u, reached 15–20 kPa above baseline values (100 kPa) during the dynamic phase of these

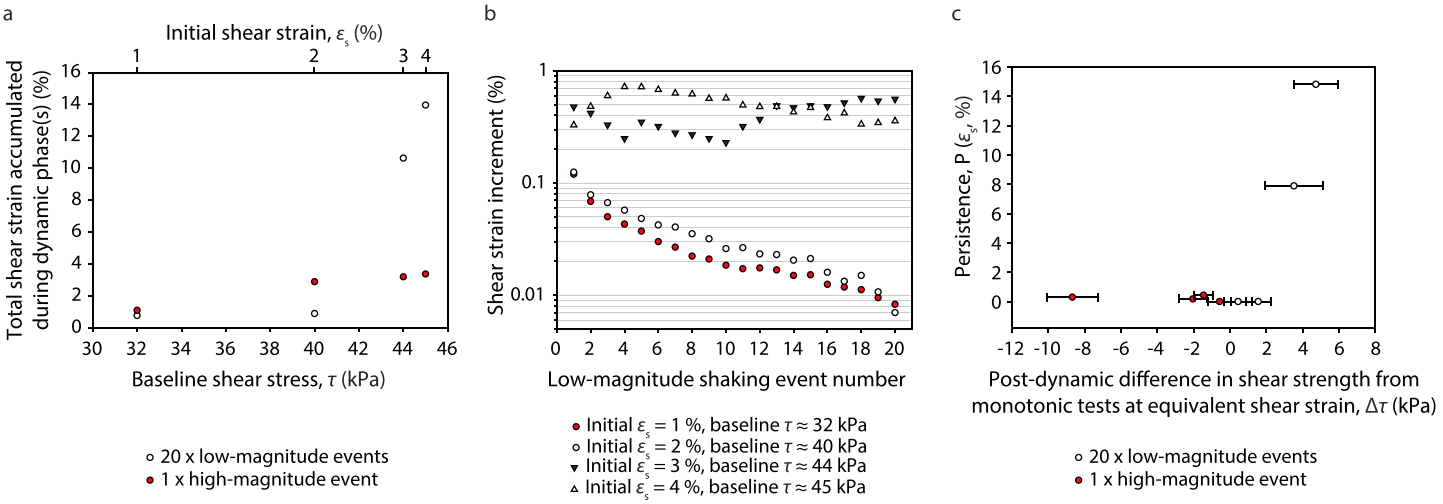

Figure 3. (a) Summary of the total shear strain accumulated during the dynamic phase(s) of each dynamic test as a function of initial shear stress values. Upper horizontal axis displays the initial shear strain at the start of the dynamic stages (indicative scale only). (b) Shear strain increments during each of the 20 low-magnitude shaking events for differing values of initial shear strain. (c) Summary of the persistence (in shear strain units) of postdynamic shear strength changes. Horizontal error bars indicate the change in postdynamic shear strength relative to the baseline shear stress envelope (best estimate and upper and lower standard deviations).

tests (Figure 2i). This prolonged undrained loading limited consolidation and ε_n during the dynamic stage. The sediment was in a less dense condition than observed under baseline conditions at equal ε_s at the end of the dynamic stage (Figures 2k and 2l). However, this dilated sediment structure did not persist (Figure 3c). During postdynamic monotonic shear, ε_n increased to equal that observed in baseline tests at equal values of ε_s (Figures 2k and 2l). This densification occurred within a ε_s increment of ~0.3% in all four high-magnitude tests (Figure 3c). Postdynamic shear strength equalled that observed in baseline monotonic tests beyond this increment, though prior to this value shear strength was lower (<10 kPa) than baseline (Figures 2i, 2j, and 3c). However, we noted subsequent minor (~1–2 kPa) weakening of the sediment relative to the baseline shear stress envelope following this initial recovery in shear strength (Figure 2i). This suggests that the lack of densification that occurs during undrained dynamic loading ultimately affects postdynamic shear strength, since the sediment is dilated relative to baseline conditions in the postdynamic phase (Figure 2l).

6. Mixed Earthquake Sequences

We assessed the influence of sequencing of shaking scenarios in two further tests, considering the effects of low-magnitude shaking prior to and following high-magnitude mainshock activity. First, we monotonically sheared one sample under displacement control until $\tau = 41$ kPa. Here equivalent ε_s is marginally less than the critical ε_s value of ~3% evident in Figure 3a. This baseline τ value is too low to permit the sample from entering unstable stress states during low-magnitude ground shaking. We subjected the sample to 20 low-magnitude shaking events (Figures 4a and 4b). The value of ε_s reached 4.2% and the sample densified during dynamic loading to a greater extent than that observed under monotonic loading (Figure 4). We immediately reestablished baseline stress conditions and then applied a single high-magnitude shaking event to the sample. The ε_s reached 5.0%: an increment of 0.8%. In comparison, where initial $\varepsilon_s = 4\%$ but where no preceding lower magnitude loading occurred, the high-magnitude shaking scenario resulted in a ε_s increment of 3.4% (>4 times greater) (Figures 3a and 4a). During postdynamic shear, the sample displayed a higher shear strength relative to baseline conditions and this persisted until $\varepsilon_s \approx 8\%$, and a weakening trend continued until $\varepsilon_s = 20\%$ (Figure 4a) as the sediment was less dense relative to baseline conditions, suggesting high sensitivity of behavior to bulk density following dynamic loading.

In the second test, we reversed the order of shaking events, beginning with a high-magnitude shaking event following monotonic shear to ~3% (Figures 4c and 4d). Undrained loading occurred and ε_n did not increase substantially during dynamic loading (Figure 4d), but the sample densified as baseline stress conditions were reestablished where $\varepsilon_s = 7.0\%$. The ε_s reached 11.5% following subsequent application of 20 low-magnitude

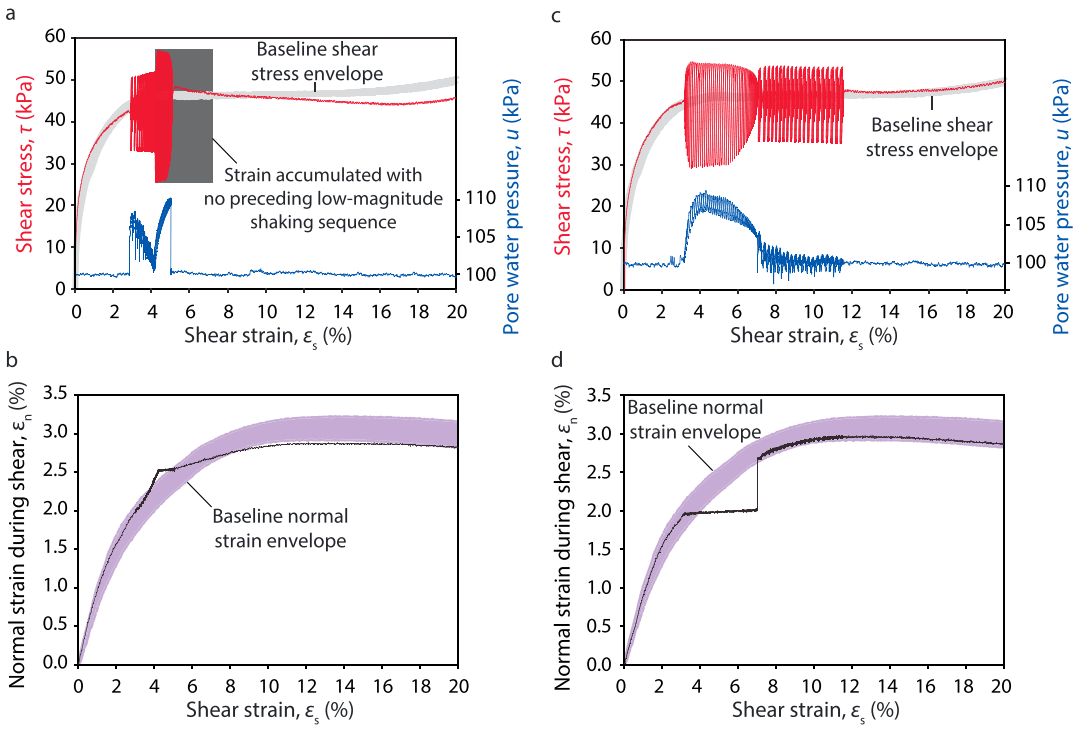

Figure 4. The influence of earthquake sequence on shear strain accumulation and volumetric behavior. (a, b) Results for behavior before, during, and following a sequence of 20 low-magnitude ground-shaking events followed by a single high-magnitude ground-shaking event. The dark grey box in Figure 4a indicates the magnitude of shear strain accumulated where initial $\varepsilon_s = 4\%$, but with no preceding low-magnitude shaking sequence. (c, d) Results for behavior before, during, and following a sequence of a single high-magnitude ground-shaking event followed by 20 low-magnitude ground-shaking events.

shaking events but did not progressively stiffen or densify (Figures 4c and 4d). Volumetric behavior throughout the dynamic stages was similar to that observed during baseline tests (Figure 4d). As such, the postdynamic strength was essentially the same as baseline shear behavior. In short, simply reversing the order of ground-shaking events resulted in a considerable difference in coseismic strain accumulation (4.3 times greater where high-magnitude precedes low-magnitude ground shaking). In addition, the postseismic shear strength also differed between the sequences tested. As such, the specific nature of earthquake sequencing can affect the stability of, and strain accumulated by landslides, in the postseismic phase.

7. Discussion

Our laboratory results highlight the importance of lower magnitude ground-shaking events in later controlling the magnitude of landslide strain accumulation during large earthquakes. Our results are most applicable to hillslope deposits of similar rheology and stress history to those tested here, indicative of shallow (~10 to 20 m depth) failures in near-surface slope materials, within which prefailure strain, manifest as ground cracking, is frequently evident. Our findings may also be applicable at the broader "landscape scale", where seismically controlled dilation controls the frictional strength of heavily damaged rock masses [*Marc et al.*, 2015; *Scheingross et al.*, 2013]. We have demonstrated that lower magnitude ground-shaking events can in some cases cause progressive densification of sediment, increasing frictional strength and reducing susceptibility to landsliding during subsequent seismicity and also in response to precipitation events. As such, our results strongly support field observations that demonstrate that focusing solely on the mainshock to understand earthquake impacts or future landslide risk may not provide an accurate assessment of hillslope or landscape response to ground shaking over coseismic and interseismic timescales [*Hovius et al.*, 2011; *Jibson*, 2011; *Keefer*, 1994]. Our data, and the mechanistic understanding of controls on material strength they provide, indicate that it is necessary to consider the effects of the sequence of events both prior to and following a

mainshock earthquake, and also in the context of hillslope rheology. These sequences and their effects may occur over timescales analogous to multiple earthquake return periods but also to the sequencing of foreshocks and aftershocks, or the relative timing and strength of seasonal monsoonal rainfall [*Lin et al*., 2008] and tropical storms [*Saito et al*., 2014].

Following large earthquakes, unfailed slopes in epicentral regions often display widespread ground cracking [*Collins and Jibson*, 2015; *Mahmood et al*., 2015; *Petley et al*., 2006]. It is important to determine the future stability of these incipient landslides for risk assessment and to project sediment fluxes and net topographic change [*Marc et al*., 2016; *Sepúlveda et al*., 2016]. Our results suggest that achieving this requires thorough knowledge of antecedent stress conditions and perturbations, and the relative timing of a ground-damaging earthquake as a component of a wider sequence of stress perturbations experienced by a slope. Our results suggest that the strengthening effects of previous lower magnitude seismic activity may increase the stability of slopes, rather than rendering them more prone to failure. Our results contest the implicit assumption that ground shaking always results in weakening of all hillslopes and leads to increases in the rate of slope failure. Furthermore, we have demonstrated that the weakening that follows a large earthquake with no antecedent foreshock activity is unlikely to persist and that shear strength will recover despite initial strain accumulation, akin to field ground cracking. By implication, ground cracking may not be a definite precursor to failure in ductile hillslope rheologies, supporting the advantages of monitoring deformation rate rather than magnitude for issuing landslide warnings [*Dixon et al*., 2015; *Intrieri et al*., 2012]. Our data support the value of monitoring earthquake-damaged hillslopes to assess whether this strengthening effect is widespread across a variety of slope settings, including those in brittle and structured materials where damage accumulation processes differ and can strongly influence slope behavior [*Brain et al*., 2014; *Clarke and Burbank*, 2010; *Parker et al*., 2015].

Assessing long-term geomorphic response to earthquakes at the landscape scale over coseismic to interseismic timescales is hindered by the relative infrequency of high-magnitude earthquakes and the limited availability of data on resultant landscape changes. As such, our understanding of both coseismic and interseismic landsliding rates and patterns is primarily empirical which potentially limits the transferability of patterns and transient rates of landsliding identified. *Marc et al*. [2015] reported an exponential reduction in elevated landslide activity and a return to preseismic landslide rates over subdecadal timescales. The four case studies considered by *Marc et al*. [2015] share broadly similar seismogenic settings, and all experienced an earthquake sequence characterized by a mainshock and a series of aftershocks. While it is effectively impossible to know the stress history of any slope, our results suggest that local fault characteristics will ultimately generate characteristic slope responses at a landscape scale evident over decades to centuries. Empirical studies documenting transient changes in landslide rates for alternative fault mechanisms are limited, particularly those that generate different earthquake sequences characterized by foreshock sequences, for example [*Hauksson et al*., 1995; *Jones and Molnar*, 1979; *Scheingross et al*., 2013; *Vidale et al*., 2001]. Fault mechanisms that generate specific and characteristic types of earthquake sequences may affect how a landscape responds to and recovers from a high-magnitude earthquake. Strong foreshock sequences may strengthen the landscape, reducing the occurrence of coseismic landsliding and limiting susceptibility to failure in the postseismic and interseismic phases. Further work is needed to better constrain the long-term geomorphic effects of, and mechanical controls on, landslides triggered by earthquakes in a range of tectonic settings where the nature and sequence of ground shaking and the stress history and density of slope-forming materials differ.

8. Summary

We have demonstrated that specific sequences of earthquakes can modify hillslope shear strength as a result of changes in material density that arise in response to ground-shaking events of different character. Critically, specific earthquake sequences can not only weaken but also strengthen hillslopes, challenging conventional wisdom. By implication, landscapes in different tectonic settings are likely to display different responses to a single earthquake due to local differences in the magnitude, frequency, and, critically, sequencing of earthquakes. Our results also reveal that coseismic changes in shear strength can endure beyond single earthquake sequences to influence hillslope susceptibility to failure during subsequent precipitation and future seismicity. This has important implications for landslide hazard assessment and in understanding and modeling landscape evolution over multiple timescales.

Acknowledgments

We are grateful for funding from the British Society for Geomorphology, NERC (NE/N007689/1) and ICL Fertilizers. We thank the Hollister Hills State Vehicular Recreation Area authorities for permitting field access; and Emma Vann Jones and Doug Smith for field assistance. We are grateful to two anonymous reviewers for their very helpful and insightful comments. Data are available on request from M.J.B. (email: matthew.brain@durham.ac.uk).

References

Brain, M. J., N. J. Rosser, E. C. Norman, and D. N. Petley (2014), Are microseismic ground displacements a significant geomorphic agent?, *Geomorphology*, *207*, 161–173.

Brain, M. J., N. J. Rosser, J. Sutton, K. Snelling, N. Tunstall, and D. N. Petley (2015), The effects of normal and shear stress wave phasing on coseismic landslide displacement, *J. Geophys. Res. Earth Surf.*, *120*, 1009–1022, doi:10.1002/2014JF003417.

Burland, J. B. (1990), On the compressibility and shear strength of natural clays, *Geotechnique*, *40*(3), 329–378.

Clarke, B. A., and D. W. Burbank (2010), Bedrock fracturing, threshold hillslopes, and limits to the magnitude of bedrock landslides, *Earth Planet. Sci. Lett.*, *297*(3–4), 577–586.

Collins, B. D., and R. W. Jibson (2015), Assessment of existing and potential landslide hazards resulting from the April 25, 2015 Gorkha, Nepal earthquake sequence, *Report Rep. 2015-1142*, 50 pp., Reston, Va.

Dadson, S. J., et al. (2004), Earthquake-triggered increase in sediment delivery from an active mountain belt, *Geology*, *32*(8), 733–736.

Dixon, N., M. P. Spriggs, A. Smith, P. Meldrum, and E. Haslam (2015), Quantification of reactivated landslide behaviour using acoustic emission monitoring, *Landslides*, *12*(3), 549–560.

Gutenberg, B., and C. Richter (1954), *Seismicity of the Earth and Associated Phenomena*, Princeton Univ. Press, Princeton, N. J.

Hauksson, E., L. M. Jones, and K. Hutton (1995), The 1994 Northridge earthquake sequence in California: Seismological and tectonic aspects, *J. Geophys. Res.*, *100*(B7), 12,335–12,355, doi:10.1029/95JB00865.

Head, K. H., and R. J. Epps (2011), *Manual of Soil Laboratory Testing Volume II: Permeability, Shear Strength and Compressibility Tests*, 440 pp., Whittles, Caithness.

Head, K. H., and R. J. Epps (2014), *Manual of Soil Laboratory Testing: Volume III: Effective Stress Tests*, Whittles, Caithness.

Hovius, N., P. Meunier, C.-W. Lin, H. Chen, Y.-G. Chen, S. Dadson, M.-J. Horng, and M. Lines (2011), Prolonged seismically induced erosion and the mass balance of a large earthquake, *Earth Planet. Sci. Lett.*, *304*(3–4), 347–355.

Intrieri, E., G. Gigli, F. Mugnai, R. Fanti, and N. Casagli (2012), Design and implementation of a landslide early warning system, *Eng. Geol.*, *147–148*, 124–136.

Jibson, R. W. (2011), Methods for assessing the stability of slopes during earthquakes—A retrospective, *Eng. Geol.*, *122*(1–2), 43–50.

Jones, L. M., and P. Molnar (1979), Some characteristics of foreshocks and their possible relationship to earthquake prediction and premonitory slip on faults, *J. Geophys. Res.*, *84*(B7), 3596–3608, doi:10.1029/JB084iB07p03596.

Keefer, D. K. (1984), Landslides caused by earthquakes, *Geol. Soc. Am. Bull.*, *95*(4), 406–421.

Keefer, D. K. (1994), The importance of earthquake-induced landslides to long-term slope erosion and slope-failure hazards in seismically active regions, *Geomorphology*, *10*(1), 265–284.

Khattak, G. A., L. A. Owen, U. Kamp, and E. L. Harp (2010), Evolution of earthquake-triggered landslides in the Kashmir Himalaya, northern Pakistan, *Geomorphology*, *115*(1–2), 102–108.

Li, G., A. J. West, A. L. Densmore, Z. Jin, R. N. Parker, and R. G. Hilton (2014), Seismic mountain building: Landslides associated with the 2008 Wenchuan earthquake in the context of a generalized model for earthquake volume balance, *Geochem. Geophys. Geosyst.*, *15*, 833–844, doi:10.1002/2013GC005067.

Lin, G.-W., H. Chen, N. Hovius, M.-J. Horng, S. Dadson, P. Meunier, and M. Lines (2008), Effects of earthquake and cyclone sequencing on landsliding and fluvial sediment transfer in a mountain catchment, *Earth Surf. Processes Landforms*, *33*(9), 1354–1373.

Mahmood, I., S. N. Qureshi, S. Tariq, L. Atique, and M. F. Iqbal (2015), Analysis of landslides triggered by October 2005, Kashmir Earthquake, *PLOS Curr. Disaster*, doi:10.1371/currents.dis.0bc3ebc5b8adf5c7fe9fd3d702d44a99.

Marano, K. D., D. J. Wald, and T. I. Allen (2010), Global earthquake casualties due to secondary effects: A quantitative analysis for improving rapid loss analyses, *Nat. Hazards*, *52*(2), 319–328.

Marc, O., N. Hovius, P. Meunier, T. Uchida, and S. Hayashi (2015), Transient changes of landslide rates after earthquakes, *Geology*, doi:10.1130/g36961.1.

Marc, O., N. Hovius, and P. Meunier (2016), The mass balance of earthquakes and earthquake sequences, *Geophys. Res. Lett.*, *43*, 3708–3716, doi:10.1002/2016GL068333.

Parker, R. N., A. L. Densmore, N. J. Rosser, M. de Michele, Y. Li, R. Huang, S. Whadcoat, and D. N. Petley (2011), Mass wasting triggered by the 2008 Wenchuan earthquake is greater than orogenic growth, *Nat. Geosci.*, *4*(7), 449–452.

Parker, R. N., G. T. Hancox, D. N. Petley, C. I. Massey, A. L. Densmore, and N. J. Rosser (2015), Spatial distributions of earthquake-induced landslides and hillslope preconditioning in the northwest South Island, New Zealand, *Earth Surf. Dynam.*, *3*(4), 501–525.

Petley, D. N., T. Higuchi, D. J. Petley, M. H. Bulmer, and J. Carey (2005), Development of progressive landslide failure in cohesive materials, *Geology*, *33*(3), 201–204.

Petley, D. N., S. A. Dunning, N. J. Rosser, and A. B. Kausar (2006), Incipient landslides in the Jhelum Valley, Pakistan following the 8th October 2005 earthquake, in *Disaster Mitigation of Debris Flows, Slope Failures and Landslides*, edited by H. Marui, pp. 47–56, Universal Academy Press, Tokyo, Japan.

Robinson, T. R., T. R. H. Davies, T. M. Wilson, and C. Orchiston (2016), Coseismic landsliding estimates for an Alpine Fault earthquake and the consequences for erosion of the Southern Alps, New Zealand, *Geomorphology*, *263*, 71–86.

Saito, H., O. Korup, T. Uchida, S. Hayashi, and T. Oguchi (2014), Rainfall conditions, typhoon frequency, and contemporary landslide erosion in Japan, *Geology*, doi:10.1130/g35680.1.

Scheingross, J. S., B. M. Minchew, B. H. Mackey, M. Simons, M. P. Lamb, and S. Hensley (2013), Fault-zone controls on the spatial distribution of slow-moving landslides, *Geol. Soc. Am. Bull.*, *125*, 473–489.

Sepúlveda, S. A., D. N. Petley, M. J. Brain, and N. Tunstall (2016), The effect of dynamic loading on the shear strength of pyroclastic ash deposits and implications for landslide hazard: The case of Pudahuel Ignimbrite, Chile, *Eng. Geol.*, *205*, 54–61.

Vidale, J., J. Mori, and H. Houston (2001), Something wicked this way comes: Clues from foreshocks and earthquake nucleation, *Eos Trans. Am. Geophys. Union*, *82*(6), 68–68.

Wang, C.-Y., C.-H. Wang, and M. Manga (2004), Coseismic release of water from mountains: Evidence from the 1999 (*Mw* = 7.5) Chi-Chi, Taiwan, earthquake, *Geology*, *32*(9), 769–772.